



University of Tennessee, Knoxville  
**TRACE: Tennessee Research and Creative  
Exchange**

---

Chancellor's Honors Program Projects

Supervised Undergraduate Student Research  
and Creative Work

---

5-2018

## **An Examination of the Au-Ni Phase Diagram for Magneto- Plasmonic Applications**

Christopher C. Walker

*University of Tennessee, Knoxville, cwalke60@vols.utk.edu*

John Carothers

*University of Tennessee, Knoxville*


Michael Roulier

*University of Tennessee, Knoxville*

Brandon Rowell

*University of Tennessee, Knoxville*

Follow this and additional works at: [https://trace.tennessee.edu/utk\\_chanhonoproj](https://trace.tennessee.edu/utk_chanhonoproj)

 Part of the [Semiconductor and Optical Materials Commons](#)

---

### **Recommended Citation**

Walker, Christopher C.; Carothers, John; Roulier, Michael; and Rowell, Brandon, "An Examination of the Au-Ni Phase Diagram for Magneto-Plasmonic Applications" (2018). *Chancellor's Honors Program Projects*. [https://trace.tennessee.edu/utk\\_chanhonoproj/2215](https://trace.tennessee.edu/utk_chanhonoproj/2215)

This Dissertation/Thesis is brought to you for free and open access by the Supervised Undergraduate Student Research and Creative Work at TRACE: Tennessee Research and Creative Exchange. It has been accepted for inclusion in Chancellor's Honors Program Projects by an authorized administrator of TRACE: Tennessee Research and Creative Exchange. For more information, please contact [trace@utk.edu](mailto:trace@utk.edu).

# An Examination of the Au-Ni Phase Diagram for Magneto-Plasmonic Applications

J. Carothers, M. Roulier, B. Rowell, C. Walker

*Department of Material Science & Engineering, The University of Tennessee, Knoxville*

**Abstract: Multiple compositions of Au-Ni alloy in a thin film were characterized for magneto-plasmonic and structural properties. Co-sputtering synthesis was employed to ensure a compositional gradient on a single Si-SiO<sub>2</sub> substrate, allowing for a range of compositions to be characterized. A gradient of 90 to 40 At % nickel was confirmed via EDS and GXR. Plasmonic properties were extrapolated from ellipsometry measurements. Annealing of the sample was performed to address metastable states and ensure the structural phases within the miscibility gap were achieved. It was shown that within the medium energy ranges of 2.6 eV to 4.2 eV (476 nm to 295 nm) plasmonic performance was at minimum maintained and often improved with the addition of up to 12.5 At % Ni. Above this nickel concentration, plasmonic properties were not improved compared to pure Au.**

## I. INTRODUCTION

### A. Thin Films

Thin films are a class of materials that possess a thickness on the order of nanometers to micrometers and are deposited or grown on a substrate. These materials exhibit many unique properties that result from the synthesis techniques employed in their production, and due to the physical scale of the film. Additionally, the nature of thin film synthesis techniques allow for a high degree of control during production, thus, the material properties can be fine-tuned based on the desired applications. Some of these unique properties include optical interference, tunneling through an insulating layer, and the enhancement of superconducting temperature and optical

absorption, as well as many others [1]. These properties make them useful in electronic, optical, and magnetic applications; both as a tool for research, and as an industry product. Their compact nature also allows for convenient integration into technological components and nanoscale devices.

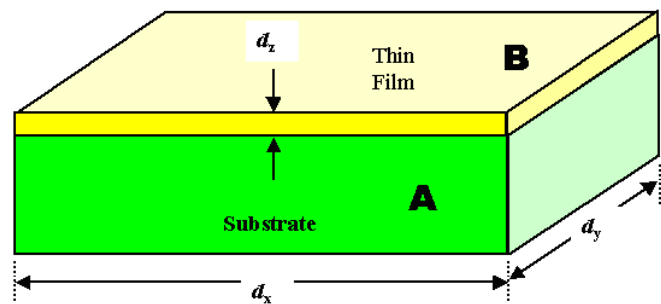


*Figure (1) - An illustration of a thin film, labeled B. The substrate, labeled A, possess dimensions  $d_x$  and  $d_y$  notably larger than the thickness of the film  $d_z$  [2].*

### B. Plasmons

Thin films allow for the application of plasmonics due to their innate ability to propagate plasmons in a functional and distinguishable manner. Plasmonics refers to the interaction between the free electrons in a metal and an electromagnetic field. Plasmons are a quantum of the plasma oscillation of free electron density with respect to the fixed positive ions in a metal. Surface plasmons are plasmons interacting at the interface of the material and dielectrics, such as metal and air. Surface plasmon resonance (SPR) shows the resonant oscillation between the negative and positive permittivity of materials stimulated by incident light. These oscillations are sensitive to any change along the interface, such as the absorption and reflection of light. Due to ohmic loss and electron-

core interactions, loss is inevitable for plasmon oscillation. Most interfaces that support surface plasmons are formed by noble metals such as gold or silver. Noble metal nanoparticles are used because of their optical properties which arise from their ability to resonate with light in the spectrum with wavelengths below 688 nm. Combining the plasmonic and magnetic functionalities of the Au-Ni system can be used to characterize the effect between localized surface plasmons and magneto-optics.

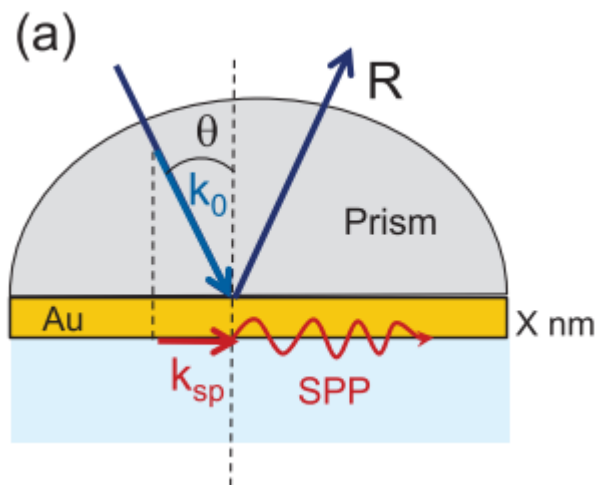


**Figure (2)** - Schematic representation of the traditional SPR configuration [3].

### C. Phase Diagram and Au-Ni System

#### 1) Au-Ni System

The Gold-Nickel system was carefully selected to fulfil the intentions of this study. Nickel being a naturally ferromagnetic metal (and thus does not propagate plasmons), provides unique attenuation effects and dispersion effects on plasmon resonances as compared to a paramagnetic or non-magnetic metal. Gold is a naturally non-reactive metal, offering stability and a free s shell electron allowing for excellent plasmon propagation. With similar electronic properties (see table 1), the two metals also show miscibility below the critical temperature. This, combined with a large miscibility gap below the eutectic point, shows promise in having favorable plasmon selectivity. The ease of sputtering was also taken into account during the selection process, as intermetallics are

**Table 1:** Relevant Properties of Au and Ni

| Property                                  | Gold, Au  | Nickel, Ni  |
|---|---|---|
| Electron Configuration                    | [Xe]4f <sup>14</sup> 5d <sup>10</sup> 6s <sup>1</sup> | [Ar]3d <sup>8</sup> 4s <sup>2</sup>                     |
| Electronegativity (Pauling)               | 2.40  | 1.91  |
| Melting Point (C)                         | 1064  | 1455  |
| Density (g/cm <sup>-3</sup> )             | 19.3  | 8.90  |
| Lattice Parameter (Å)                     | 4.0782  | 3.524   |
| Ionization Energy (kJ mol <sup>-1</sup> ) | 1 <sup>st</sup> = 890.128<br>2 <sup>nd</sup> = 1949   | 1 <sup>st</sup> = 737.129<br>2 <sup>nd</sup> = 1753.027 |
| Atomic Radius (Å)                         | 2.14  | 1.97  |

unfavorable at temperatures below the 810 °C critical point, with lattices that are both FCC. The difference in lattice parameters (352.4 pm, 407.82 pm for Au and Ni) allows for obvious separation between compositional phases.

#### 2) Phase Diagram

There are two areas of interest in the Au-Ni system (Figure 3): the  $\alpha_1$  and  $\alpha_2$  miscibility region and the single phase region below the eutectic point. Below 810 °C a gold rich phase and a nickel rich phase exist in equilibrium,  $\alpha_1 + \alpha_2$ . The  $\alpha_1$  structure corresponds to a Au rich composition with small Ni dopants in the unit cell structure. The  $\alpha_2$  structure corresponds to a Ni rich composition with

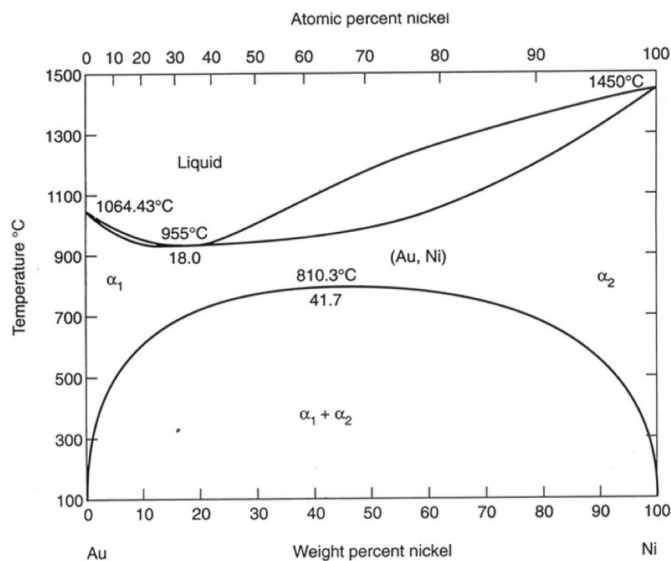


**Figure (3)** - Binary phase diagram of the Au-Ni system [4].

small Au dopants in the unit cell structure. Within the miscibility region, each concentration will form grains proportional to the total atomic composition percentage of the system, whereas within the individual grain structure, small inclusions of the lesser proportion element will separate into inclusions within the  $\alpha_1$  or  $\alpha_2$  structures respectively. Above the miscibility region and below the eutectic point, a single phase will form with an effective mixing of the elements into a single phase FCC structure at the respective overall composition. This region exists due to a metastable energy barrier preventing atomic diffusion kinetics from phase separating. The ability for a Au rich structure to exist with ferromagnetic Ni inclusions prevents the Ni from completely quenching the plasmonic activity of the Au system and allows magnetic influence on the plasmonics.

#### D. Applications of Plasmons

The inclusion of the ferromagnetic element Nickel was chosen specifically to reduce surface plasmon polariton (SPP) evanescent effects. This is due to the inherent influence a magnetic field has on the magnitude of plasmon polaritons. In simple terms, pure noble metals have desirable resonance effects, but lack broad magneto-optical activity. Ferromagnetic doped metals offer the opposite; highly active magneto-optical effects, with broad spectrum plasmon resonances. Broad spectrum means that the incident angle for surface plasmon generation covers a wide range, preventing the

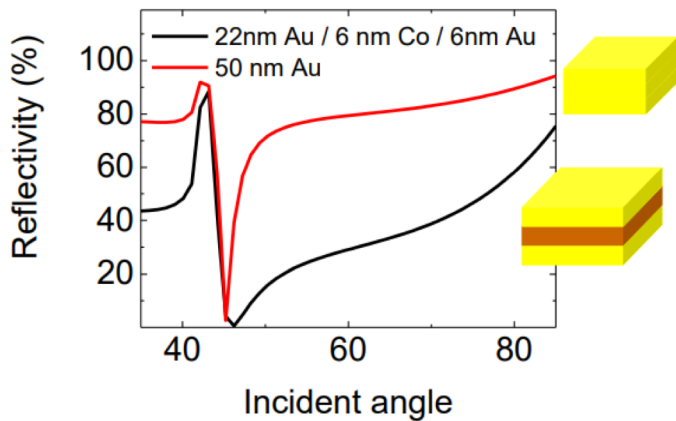


**Figure (4)** - Illustrates the local minimum of percent reflectivity as a function of incident angle of light. Application of a ferromagnetic material shows the broadening of the range of plasmon interaction [5].

accurate selection of specified sample interaction. Because plasmon excitation can happen over a range of incident light, reflectivity is typically used as a plasmon indicator. When reflectivity reaches a local minima, it correlates to a generated plasmon interaction within a sample. This is determined by the reflectivity equation (equation 1). This effect is compared for ferromagnetic vs. pure noble metal thin films in (Figure 4).

$$R = 1 - \frac{4\gamma_i\gamma_r}{(k_0n_p \sin(\theta) - k_{sp})^2 + (\gamma_i + \gamma_r)^2} \text{ Eq. 1 [3]}$$

where  $R$  is the reflectivity and  $\gamma_i$  and  $\gamma_r$  are the SPP absorption and radiation damping coefficients.

The addition of a ferromagnetic changes the magnitude of the wave vector, making plasmon interaction more pronounced and increasing experimental sensing precision. When a magnetic field is applied perpendicular to the propagation direction and parallel to the substrate surface, it acts to increase the magnitude of the plasmon wave vector as given in the functions:

$$k_{sp} = k_0n_p \sin(\theta) \text{ Eq. 2 [3]}$$

$$k_{sp} = k_0n_d \sqrt{\frac{\epsilon_m}{\epsilon_m + n_d^2}} \text{ (ferromagnetic) Eq. 3 [3]}$$

where  $k_0$  is the wave vector of light in vacuum,  $n_d$  the refractive index of the dielectric material and  $\epsilon_m$  is the dielectric constant of the metal. Most sensors that take advantage of this method rely on the change in incident vs. refracted light inducing different SPP magnitudes. The interactions of these varying SPPs with known incident light (typically selected through slit geometry) is known as the change in measured output as a function of the dielectric constant. This means that the measurement sensitivity can be correlated with the dielectric constant as:

$$S = \frac{\delta O}{\delta k_{sp}} \cdot \frac{\delta k_{sp}}{\delta n} + \frac{\delta O}{\delta k_m} \cdot \frac{\delta k_m}{\delta n} \text{ Eq. 4 [3]}$$

where  $O$  is the change in optical sensitivity for sensors and  $k_m$  represents the change in the magnetic field induced modification of the SPP wave vector.

All of the above principles are used to optimize the ability of SPPs to propagate and interact with the measurement medium. The uses vary widely and includes biosensors, ultra fast communication, high density memories, and high efficiency solar energy harvesting.

## II. METHODOLOGY

### A. Sputtering Process

The properties of thin films are dependent on the method used to synthesize them. These techniques employ either chemical (such as chemical vapor deposition) or physical methods (such as lithography) to deposit the film. One useful physical deposition technique is known as sputtering. This process can be used for the creation and deposition of elements with atomic level precision as individual atomic species are generated and transported to the receiving substrate. The sputtering apparatus contains a high vacuum chamber that is backfilled typically with an inert process gas, such as argon. This chamber houses a source that contains the target material (material to be deposited as a film) which acts as a cathode and a substrate, which acts as an anode. Power is applied to the source and at an appropriate pressure will ignite a plasma where the cathode develops an applied negative voltage and the ionized gas generates a current. These positively charged gas ions are accelerated toward the negatively charged source, where they will strike the target. During this collision a target atom may be ejected with the reflected trajectory of the incident ion. A portion of these target atoms strike the substrate and are deposited as a film. The rate of deposition of the film is dependent on the total power (watts) on each target. Therefore, different powers may be selected for each material to create varying deposition proportions. The deposition thickness is dependent on the sputtering time.

This method was employed to produce a thin film

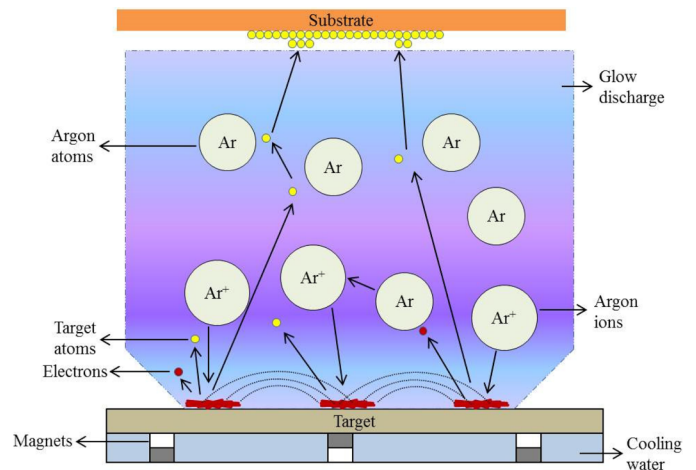


**Figure (5)** - An illustration depicting the sputtering process using Ar as a process gas. The target atoms are dislodged by the free electrons and are subsequently collected on the substrate [6].

of the Au-Ni system on a Si-SiO<sub>2</sub> substrate. The substrate was statically mounted so that composition varied as a function of position. Au:Ni have a 3:2 atomic volume ratio, thus 20 W and 70 W of power were applied to each target to yield a deposition rate of 3 nm and 2 nm per minute respectively. Argon served as the ionizing gas at a pressure of 25 mtorr for the duration of the sputtering. Total deposition time of one hour was selected for a film thickness of 300 nm. This process created in effect as a representation of the binary phase diagram for these metals at room temperature.



**Figure (6)** - The interior of the sputtering chamber. The orange target on the left is Au and the purple target on the right is Ni..



## B. Annealing

Annealing is the heat treatment of a material to induce changes in the physical and chemical properties of said material. In the Au-Ni system, annealing below 810 °C will change the physical structure without changing the chemical composition. As temperature increases, the ratio of gold to nickel stays the same but the amount of nickel in the gold rich  $\alpha_1$  phase and the amount of gold in the nickel rich  $\alpha_2$  phase decreases. This structural change created by annealing allows for the study of the plasmonic properties of multiple structures from one sample.

### 1) Au-Ni Thin Film Annealing

Annealing was performed inside the sputtering chamber after initial testing was completed on the sample. The chamber was held at vacuum and the sample holder was heated to 600 °C for one hour. A thermocouple reading the chamber temperature was placed at the interface of the sample plate and the sample to minimize the temperature variability.

## C. SEM & EDS

A scanning electron microscope (SEM) is a type of spectroscopy that produces images of a sample by bombarding the surface with a focused beam of electrons. The electrons interact with atoms in the sample producing scattering and emission effects that indicate the sample's topography and composition. The advantage of SEM allows the characterization of structures and features on orders of magnitude below the physical limitations of optical microscopy. Energetic electrons have

nanometer scale wavelengths, and the focus is limited by the area of the beam, which approaches resolutions of <10nm. Backscattered electrons in the SEM display compositional contrast that result from different Z value elements. Energy Dispersive Spectroscopy (EDS) detects characteristic x-rays generated via inelastic collisions of the primary electrons and core level electrons of the atoms in the solid. This technique allows identification of the particular elements in the material and their relative proportions. This technique can be extrapolated to verify the composition, stoichiometry, and contaminants of thin films. Both of these methods were leveraged to verify the composition and gradient direction of the sputtered sample.

## D. X-ray Diffraction Characterization

X-rays are a type of electromagnetic radiation on the order of ~.01 to 10 nm. To produce x-rays, high energy electrons are bombarded against a target material. This material determines the wavelength of generated x-rays and is chosen to maximize sample interaction. The x-rays produced are filtered, polarized and directed incident to the sample. The intensity of the then reflected and diffracted rays are measured and normalized against the incident beam. Using this method, crystallographic properties of a sample can be measured by observing the relative intensities of reflected waves as a function of  $2\theta$ . These properties include elemental composition, lattice parameter, unit cell structure, orientation, and phase fractions. The values for which are determined using  $R^2$  fitting of the data to theoretical models yielding statistically supported values.

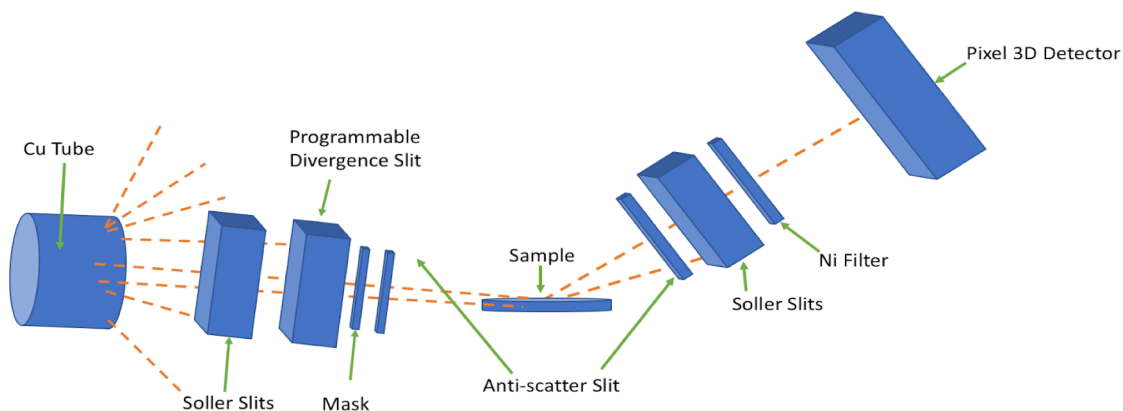


Figure (7) - Schematic of Bragg-Brentano diffractometer system.

Given the inherent limitation of thin films, grazing angle x-ray diffraction (GXRD) was required to prevent substrate interactions with the diffracted beam. Multiple measurements were taken across the gradient of the Au-Ni film to confirm compositional phase transitions, and compare the  $\alpha_1$  and  $\alpha_2$  phase fractions. Approximately 2% of the area of the sample was measured at each position due to the low grazing angle geometry (Figure 7).

### E. Ellipsometry and Reflectivity

Ellipsometry determines a material's optical properties based upon how that material behaves across the electromagnetic spectrum. Light is composed of two waves which are oriented orthogonally to the direction of propagation. These waves have the same properties as any other wave, namely: an amplitude, frequency, and phase.

One characteristic that this technique leverages is the polarizability of light. This means that the amplitude and phase of each light wave may be chosen to exhibit certain propagation parameters. With these values controlled, certain effects can be predicted and measured as the light interacts with the target.

While the phase differences of two waves of light determine whether they will constructively or destructively interfere, the amplitudes determine orientation. Thus, when both amplitude and phase aspects of light are altered, the resulting "image" on the x,y plane becomes an ellipse. (polarized light has an "image" of a line, out of phase light is a circle). This is where the name ellipsometry comes from, as it is this change in wave properties that are quantified. Another important behavior to note is that as light enters a material, the wavelength will attenuate, whereas the frequency will stay the same. This rate of extinction is unique to every material. It is also influenced by the energy of the light incident to the material, i.e. some materials absorb light at different wavelengths. The technique of ellipsometry uses the known incident light and compares it to the reflected and refracted light of the resulting beam. Mechanically, the detectors

within this technique leverage the specularity of the light (angle incident = angle reflection) to isolate a

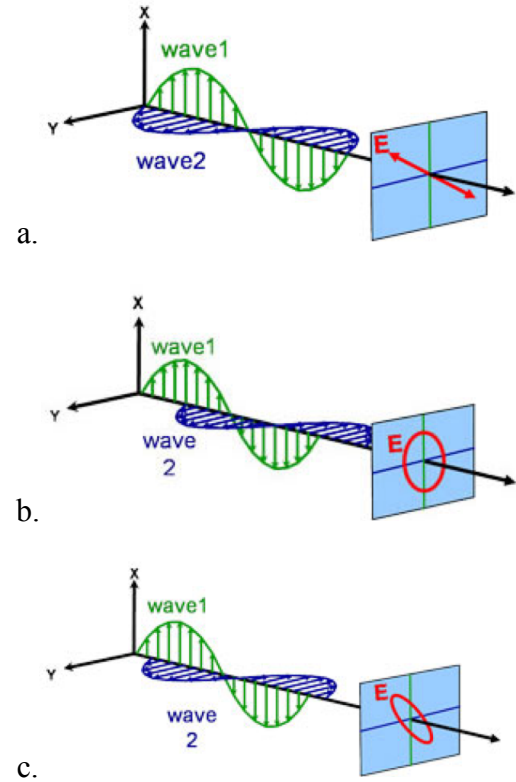


Figure (8) - a) normal, in phase light b) circular light c) elliptical light [7].

plane of incidence for the sample. It is important to note that special considerations must be taken into account if the sample is anisotropic. For the purposes of this study, thin films are considered isotropic. Once the light has been reflected, refracted, changed phase, and/or amplitude, it is collected in the detector of the device. The detector measures the values for the amplitude, known as  $\Psi$ , and phase, known as  $\Delta$ . They are then compared to the original incident values, and a ratio is extrapolated. This ratio is known as the complex reflectance ratio as denoted by:

$$\rho = \tan(\Psi) e^{i\Delta} \quad \text{Eq. 5}$$

$\rho$  = the complex reflectance ratio  
 $\Psi$  = measured change in amplitude  
 $\Delta$  = phase shift [7]

While  $\Psi$  and  $\Delta$  do not have physical significance, the values for  $\Psi$  and  $\Delta$  are used to limit a regression model, where the variables of interest such as the dielectric constant or thickness are iterated until a reasonable  $R^2$  value is obtained. The variables are

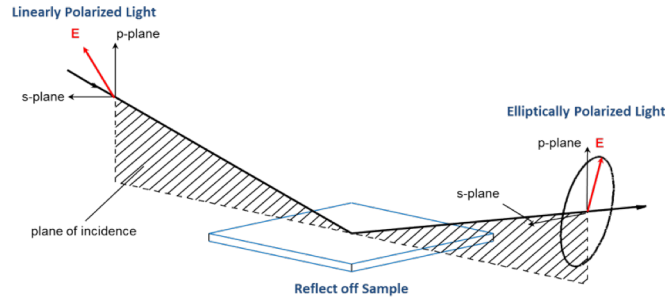


**Figure (9)** - Model of ellipsometry experimental setup for incident and reflected light [7].

only limited to the number of measured values, so any two properties which are effective on incident light may be modeled. Specifically, for thin film thickness values the  $\Delta$  value is most important, as broad interference limits the reflected intensity accuracy. However, changes in phase are variant and are sensitive to atomic layers; this is why thicknesses below the wavelength of incident light are still quantifiable. Overall, this technique gives real usable limits for modeling properties and behaviors of thin films in the optical and electronic spectra; particularly  $n$  and  $k$ , which are the refractive index and dielectric constant respectively. The refractive index,  $n$  is defined as:

$$n = \frac{c}{v} \quad \text{Eq. 6}$$

where  $c$  is the speed of light in a vacuum and  $v$  is the phase velocity a medium. The dielectric constant  $k$  is defined as:

$$k = \frac{C}{C_0} \quad \text{Eq. 7}$$

where  $C_0$  is the capacitance of two plates with a vacuum between them and  $C$  is the capacitance of two plates with a dielectric in between them with a dielectric constant  $k$ .

For the Au-Ni thin film, nine ellipsometry measurements were taken across the gradient of the

sample, yielding varying  $n$  and  $k$  values in proportion to the compositional gradient. Note that the data received corresponded to the  $\epsilon_1$  and  $\epsilon_2$  values within the optical property equations and thus were converted to  $n$  and  $k$  via equations 8-10.

$$\epsilon_c = \sqrt{\epsilon_1^2 + \epsilon_2^2} \quad \text{Eq. 8}$$

$$n = \sqrt{\frac{\epsilon_c + \epsilon_1}{2}} \quad \text{Eq. 9}$$

$$k = \sqrt{\frac{\epsilon_c - \epsilon_1}{2}} \quad \text{Eq. 10}$$

where  $\epsilon_c$  is the complex component calculated from  $\epsilon_1$  and  $\epsilon_2$ .

## F. Instrument Parameters

**Table 2:** Parameter values for SEM, EDS, and GXRD.

| Parameter               | Value          |
|-------------------------|----------------|
| SEM Image Voltage       | 20 keV         |
| EDS Scan Voltage        | 10 keV         |
| EDS Scan Current        | 1000 mA        |
| Grazing Angle           | 4.0°           |
| X-ray Source            | Cu Ka 1.54 Å   |
| X-ray Voltage / Current | 45 keV / 40 mA |
| Line scan dimensions    | 12 x 0.4 mm    |
| Divergence slit         | 1/32° Fixed    |
| Step Size               | .03°           |
| Ellipsometry Energy     | 0.8 - 5 keV    |



### III. RESULTS & DISCUSSION

#### A. EDS

Key results in the graph from EDS are the characteristic peaks for Ni and Au at 0.85 keV and 2.1 keV (Figure 10). The presence of the peaks, and the lack of additional prominent peaks indicates the sample was largely free from impurities. Evidenced by the observation of Si (1.6 keV) and O (0.52 keV)

peaks with insignificant counts (intensities), indicated the intended sample composition and purity was achieved. The decreasing trend of the characteristic Au peak intensity as a function of increasing Ni content is evidence for the confirmation of a compositional gradient across the substrate. Similar behavior but with increasing intensity was observed for the characteristic Ni peak, leading to the same conclusion.

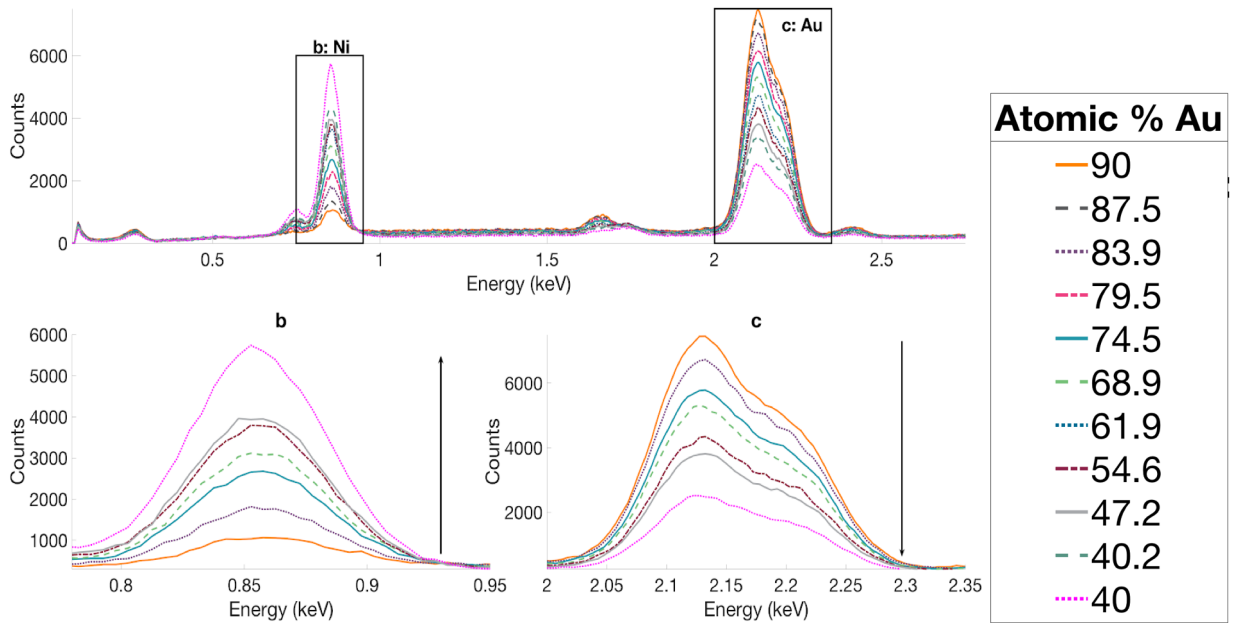


**Figure (10)** - Full spectrum of EDS data, b) shows Ni peak at 0.85 eV c) shows Au peak at 2.1 eV

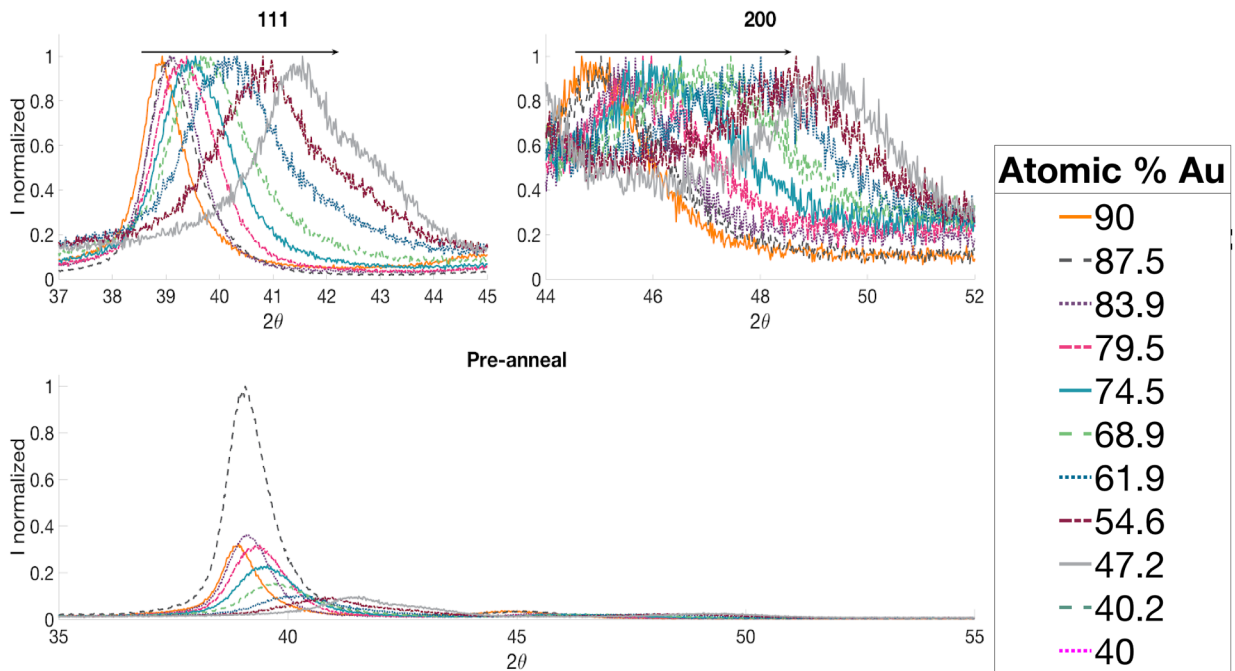


**Figure (11)** - XRD spectrum from 35°- 55° 2θ of pre-annealed film. (111) and (200) reflections have been normalized to illustrate the shift in peak position.

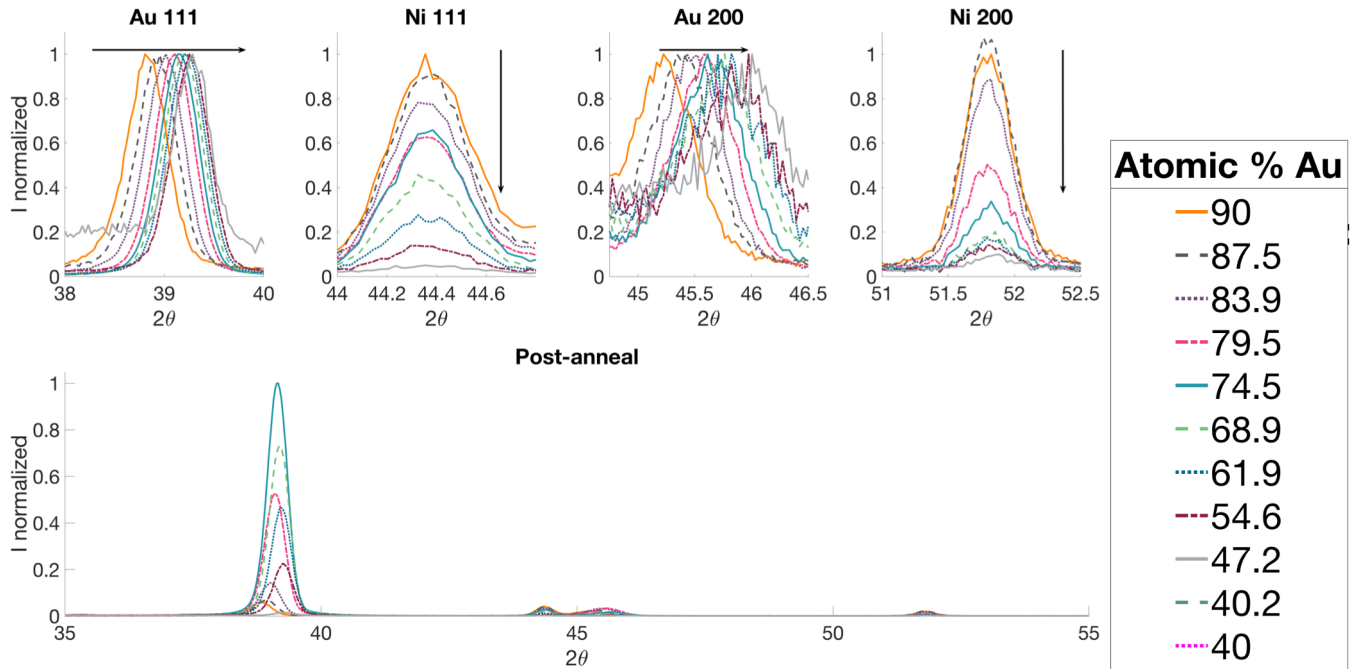


Figure (12) - XRD spectrum from 35°- 55° 2θ of post-annealed film.

## B. GXRD

### 1) Pre-anneal

Preliminary GXRD on the compositional gradient before annealing revealed the presence of two FCC reflections: (111) and (200) between 35 and 55 2θ. With full Au  $\alpha_1$ -Ni  $\alpha_2$  separation, each constituent behaves as its own FCC structure due to the difference in lattice parameter between the two compositions. This dictates the presence of representative Au rich and Ni rich (111) and (200) reflections that were not observed. This is indicative of incomplete phase separation between the  $\alpha_1$  and  $\alpha_2$  constituents and proves that the gradient is in a metastable structural state post sputtering. This metastable state is similar to the structure experienced at 850 °C (see figure 3) and results from the sputtering process limiting the phase separation kinetics during film formation. The (111) and (200) peaks experienced a rightward 2θ shift of 2.716° and 4.463° respectively. The full width-half max (FWHM) of the (200) peak increased as a function of 2θ and is influenced by background scattering and other fundamental properties of GXRD.

### 2) Post-anneal

Post-anneal GXRD analysis indicated multiple

reflections for the (111) and (200) planes. This verifies that the metastable nature of the film was diminished with heat treatment, and that separation of the  $\alpha_1$  and  $\alpha_2$  constituents was achieved. Rightward shifts in peak 2θ were observed in the normalized Au peaks indicating a decrease in lattice parameter as at% Ni increased (Figure 12). The Ni peaks were not normalized due to a downward shift in intensity, corresponding to a higher concentration of Ni. A cause correlation was not explored for this intensity behavior.

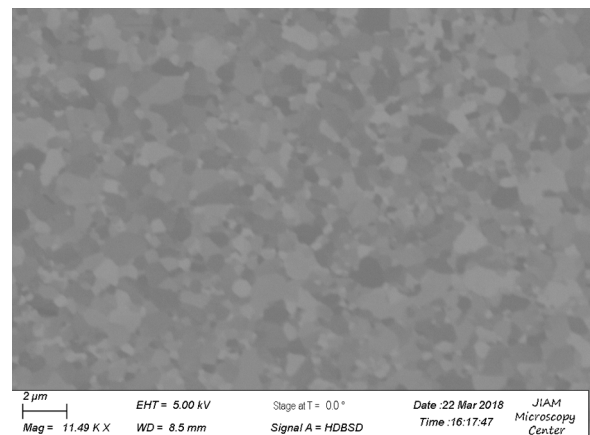


Figure (13) – SEM image of  $\alpha_1$  and  $\alpha_2$  separation at 90 at% Au.

### C. EDS vs. XRD Comparison

Both the EDS and XRD data confirm that the composition changes as a function of position on the sample. The data points in Figure 13 show the observed and calculated composition at each point. Linear trendlines have been calculated and overlaid with the data to show the decreasing Au concentration. Comparison of the trends verifies the compositional gradient as both have  $R^2$  values of at least 0.97.

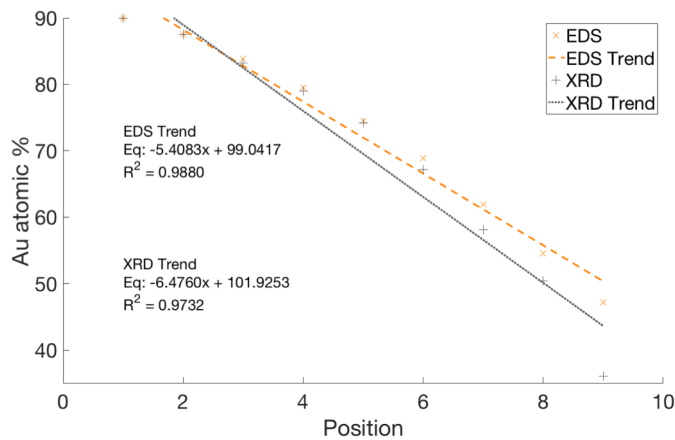


Figure (14) – Comparison of compositional trends of EDS and XRD data.

### D. Ellipsometry

#### 1) Pre & Post Anneal

The initial ellipsometry results provided data for  $\epsilon_1$  and  $\epsilon_2$  as a function of applied energy (in eV). These quantities were converted to  $n$  and  $k$ , then plotted against the values for pure Au and pure Ni. The resulting graphs are listed in Figure 15. As a comparison to the post-anneal data, the pre-anneal results had higher variability and exhibited incoherent behavior attributed to the metastable state of the film. It should be noted that the data did not follow the expected behavior of the system, without any outlying or extraneous results. No single composition in the pre-anneal analysis displayed improvements simultaneously for  $n$  and  $k$ , with only a marginal increase in both values over differing energy ranges. The post-anneal data exhibited a slight increase in performance of the refractive index above the 2.5 eV mark, and an improvement in the dielectric constant from 2.6 to 3.8 eV (Figures 16, 17 respectively). Within the 2.6 to 3.8 eV range, the data suggests reduced plasmon attenuation and increased energy conversion as compared to pure Au. These improvements were only present for compositions up to the 12.5 at% Ni.

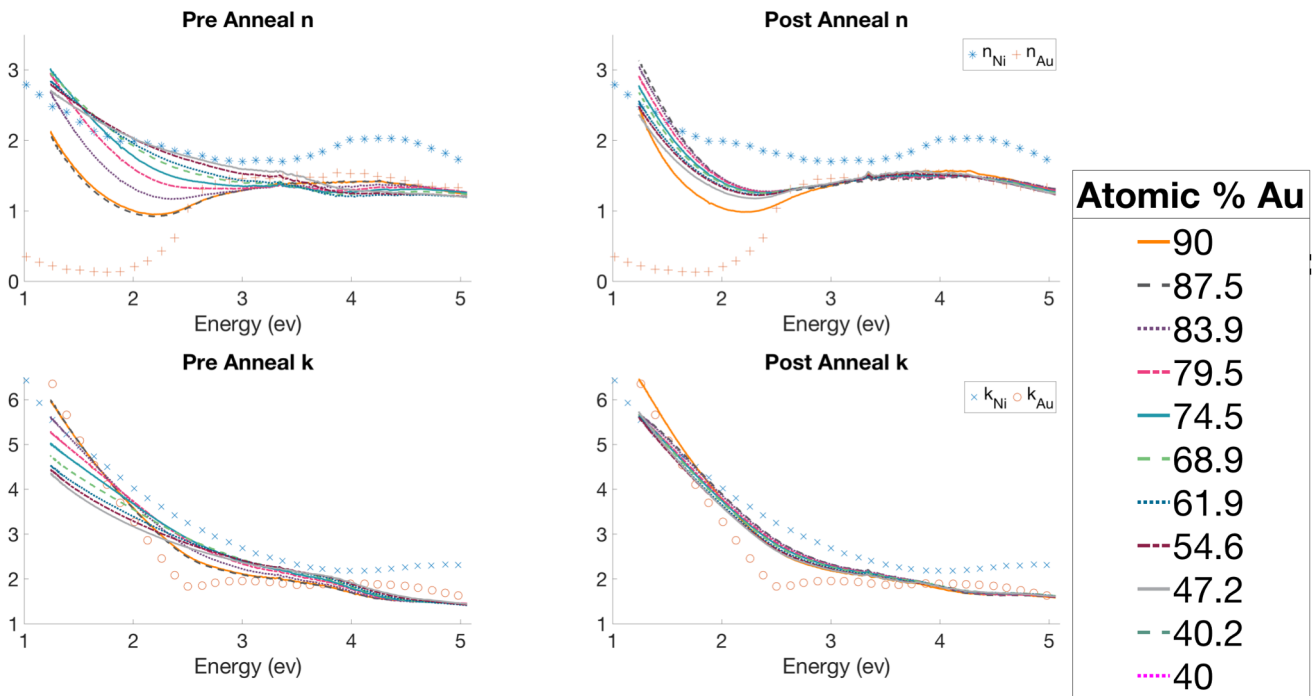


Figure (15) - Pre and post annealed  $n$  and  $k$  values. Improved performance is denoted by a decrease in  $n$  and an increase in  $k$  compared to pure Au.

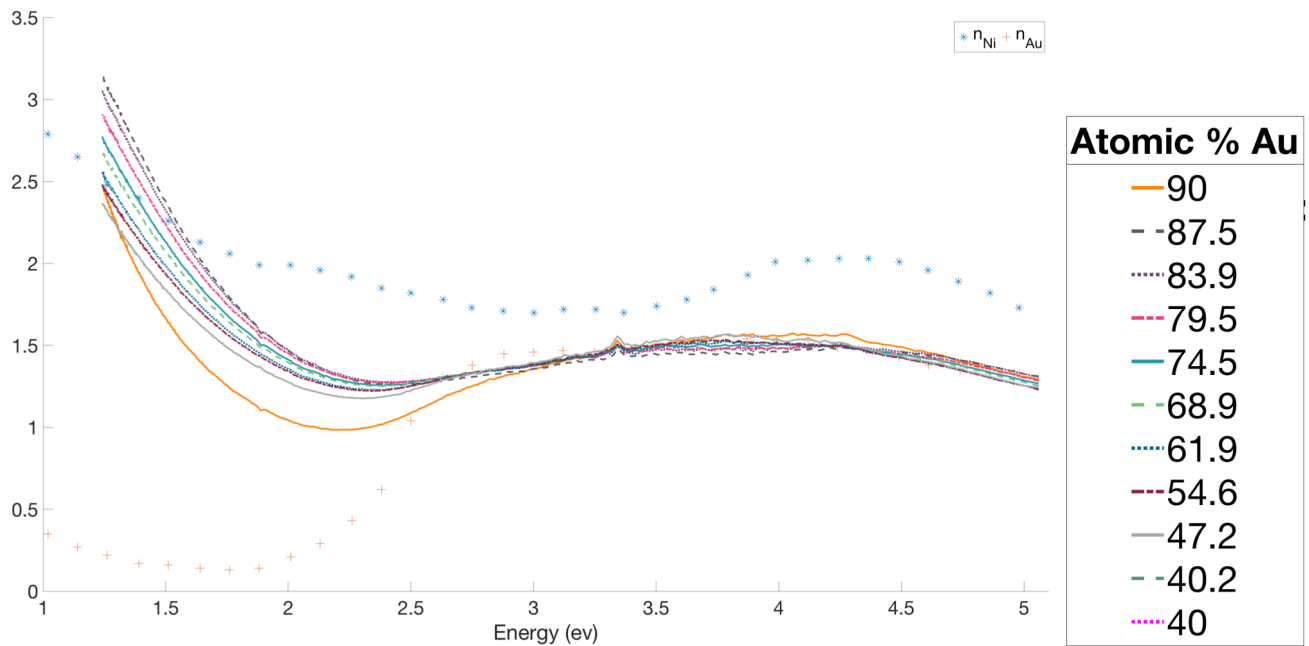


Figure (16) – Post anneal data for  $n$ , the refractive index.

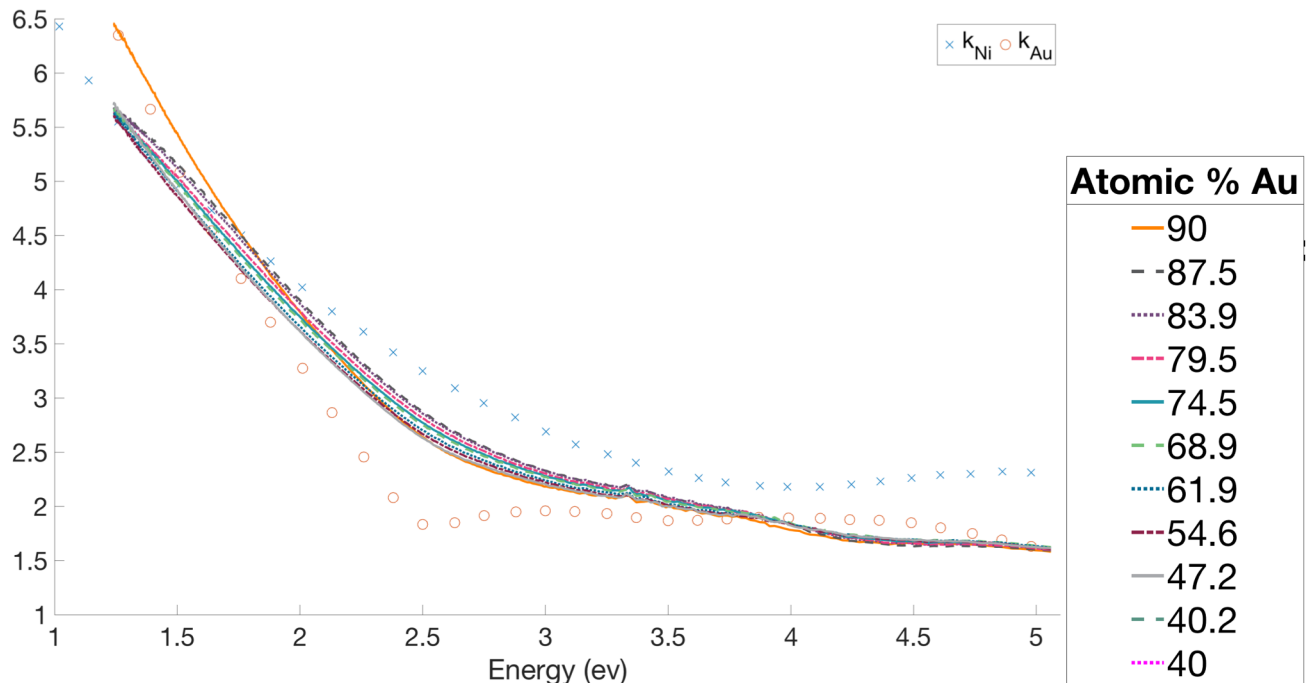


Figure (17) – Post anneal data for  $k$ , the dielectric constant.

At doping concentrations above 12.5 at% Ni, a trend of decreasing performance was observed for both  $n$  and  $k$  in post and pre-annealed data.

#### IV. CONCLUSION

A comprehensive review of the data strongly indicated that improved plasmonic performance in the energy range of 2.6-3.8 eV was achieved with the addition of up to 12.5 at% Ni in a Au thin film.

The processing required for such results included a co-sputtering synthesis technique and a post anneal to eliminate any metastable phase constituents within the system. The creation of the Ni dopant gradient was paramount in the observation of ferromagnetic influence on the optical properties of a plasmonically active metal within the medium to high energy ranges. In cases of medium energy range applications (around 3eV), plasmonic attenuation and activation energies were shown to

decrease with a Ni dopant, resulting in an increase in applied device sensitivity and efficiency. This suggests that the use of a ferromagnetic dopant within a noble metal plasmonic system, such as in optical sensors or energy harvesting devices, can reduce manufacturing costs without sacrificing device performance.

## V. FUTURE RESEARCH

The focus of this project was to characterize the optical properties (plasmonics) of the Au-Ni system as a function of composition. The ferromagnetic nature of Ni can provide enhanced plasmonic properties, thus, characterizing its magnetic effects would be useful. PPMS and Magnetometry can be utilized to study the magnetic contributions of Ni in a Au-Ni thin film.

### A. PPM

PPMS (physical property measurement system) is an analytical instrument that can measure a variety of electrical and magnetic properties. These measurements include: vibrating sample magnetometry, AC susceptibility measurements, torque magnetometry, AC electrical transport, DC resistance measurements, and heat capacity.

### B. Magnetometry

Magnetometry is an investigative technique that measures the magnetization (magnetic moment) of a material to determine its magnetic ordering as a function of temperature and an applied field. It can also measure any phase transition associated with a change in magnetic ordering.

### C. Additional Research

Due to the well characterized magneto-plasmonics of the Au-Co system, useful data could be extracted from a comparison experiment between Au-Co and Au-Ni, using the same parameters as the experiment presented in this paper. An economic study of replacing Au with up to 12.5% Ni in current magneto-plasmonic applications could also be completed. This would help determine the engineering value of this system in regards to cost vs. performance.

## VI. ACKNOWLEDGMENTS

Thank you to Dr. Rack, Dr. Fowlkes, and David Garfinkel for the opportunity to work on this project and helping us throughout. Thank you to Michael Koehler for his assistance with GXRD calculations and acquisition. We appreciate the support of the JIAM facilities.

## VII. REFERENCES

- [1] K. L. Chopra and I. Kaur, *Thin Film Device Applications*. New York: Plenum Press, 1983.
- [2] H. Föll. *Semiconductor Technology - Adhesion*.
- [3] D. Martin-Becerra, G. Armelles, M. U. Gonzalez, and A. Garcia-Martin, "Plasmonic and magnetoplasmonic interferometry for sensing," *New Journal of Physics*, 2013.
- [4] T. Yang, C. Manuel, R. d. Almeida, D. Ramasamy, F. José, and A. Loureiro, "A detailed study of Au-Ni bimetal synthesized by the phase separation mechanism for the cathode of low-temperature solid oxide fuel cells," *Journal of Power Sources*, vol. 269, 2014.
- [5] A. Garcia-Martin, "Magnetoplasmonics: Fundamentals and Applications," 2008.
- [6] D. K. Maurya, A. Sardarinejad, and K. Alameh, "Recent Developments in R.F. Magnetron Sputtered Thin Films for pH Sensing Applications—An Overview," *Coatings*, vol. 4, pp. 756-771, 2014.
- [7] J. A. Woollam. (2017). *Ellipsometry Data Analysis*.